# Cell size control driven by the circadian clock and environment in cyanobacteria

Bruno M.C. Martins[1], Amy K. Tooke[1], Philipp Thomas[2*], James C.W. Locke[1**]

[1]Sainsbury Laboratory, University of Cambridge, Bateman Street, Cambridge CB2 1LR, UK

[2]Department of Mathematics, Imperial College London, 180 Queen's Gate, London SW7 2AZ, UK

[*]*Email*: philipp.thomas@imperial.ac.uk

[**]*Email*: james.locke@slcu.cam.ac.uk

**Abstract**

How cells maintain their size has been extensively studied under constant conditions. In the wild, however, cells rarely experience constant environments. Here, we examine how the 24-hour circadian clock and environmental cycles modulate cell size control in the cyanobacterium Synechococcus elongatus using single cell time-lapse microscopy. Under constant light, WT cells follow an apparent sizer-like principle. Closer inspection

reveals that the clock generates two subpopulations, with cells born in the subjective day or night following different division rules. A stochastic model explains how this behaviour emerges from the interaction of size control with the clock. Combining modelling and experiments, we go onto show how under physiological light-dark cycles, the clock shifts cell division away from dusk and dawn, causing division to occur in more energetically favourable conditions.

## Introduction

Organisms control the size of their cells [1–5]. In growing cell colonies or tissues they must do this by deciding when to divide. The principles of cell growth and division in microorganisms have been studied for many years [6,7]. Multiple size control principles have been proposed, including the sizer model, where cells divide at a constant size irrespective of birth size, or the timer model, where cells grow a specific time before dividing [8–14]. Recent time-lapse analysis of microbial growth at the single cell level suggested that bacteria often follow an 'adder' or 'incremental' model [15–20], where new-born cells add a constant cell length before dividing again. This principle allows cell size homeostasis at the population level [14,17].

Although the rules of cell division under constant conditions are being elucidated, cell division in many organisms is controlled by intracellular cues and time-varying environmental signals. For example, cell division and growth are tightly linked to light

levels in algae [21–23], while growth is enhanced in the dark in plant hypocotyls [24]. The Earth's cycles of light and dark can thus cause 24h oscillations in cell division and growth. To anticipate these light-dark cycles many organisms have evolved a circadian clock which drives downstream gene expression with a period of 24h [25]. The circadian clock has been shown to gate cell division to particular times of day in many systems, from unicellular organisms [26,27] to mammals [28–30]. It remains unclear how and why the clock modulates the innate cell growth and division principles that organisms follow.

The cyanobacterium *Synechococcus elongatus* PCC7942 is an ideal model system to address the question of how cell size homeostasis can be controlled and modulated by the circadian clock and the environment. Cells are directly coupled to the environment as ambient light levels modulate growth [31], which can be monitored in individual cells over time [32–34]. An additional advantage is that the key components of the circadian clock in cyanobacteria are well characterised. The core network consists of just three proteins (KaiA, KaiB and KaiC) that generate a 24-hour oscillation in KaiC phosphorylation [35–37]. The state of the clock is then relayed downstream to activate gene expression by global transcription factors such as RpaA [36,38]. Many processes in *Synechococcus elongatus* are controlled by its circadian clock [36,38–40], including the gating of cell division [27,33,41]. The prevalent idea is that cell division is 'allowed' at certain times of the day (gate open) and restricted at others (gate closed).

Gating of cell division in Synechococcus elongatus was first demonstrated by Mori et al. under constant light conditions [27]. They showed that cell division was blocked in the subjective early night, but occurred in the rest of the day and night. Single cell time-lapse studies under constant light conditions have further examined the properties of gating, and have suggested a mechanism for it [33,41]. Elevated ATPase activity of KaiC has been proposed to inhibit FtsZ ring formation through a known clock output pathway [33]. It remains unclear what the function of this gating is, although proposedly gating can increase the fidelity of the clock [33]. It also remains unclear what effect the coupling of the clock to cell division has on cell size homeostasis for Synechococcus elongatus, and what are the underlying division rules.

In this work, we examine how the environment and the clock modulate cell size control in *Synechococcus elongatus* using single cell microscopy (Fig. 1). In the wild type (WT), the clock splits cells into two subpopulations following different division rules. Cells born during subjective night add less length before dividing again, allowing them to divide before the end of the day, whilst cells born during subjective day add more length, avoiding dividing in subjective night. We develop a stochastic model that explains these cellular decisions. To understand the significance of these results we examine growth and division under more physiologically relevant graded light-dark cycles. Combining modelling and experiment, we find that the clock gates division of fast dividing cells away from dusk, and slow dividing cells away from dawn. This could provide a functional

benefit, by avoiding division occurring during times where growth arrest could occur due to darkness [42].

## Results

### The circadian clock generates two subpopulations following different growth rules under constant light conditions

To examine the role of the clock in cell size control in *Synechococcus elongatus*, we first studied growth and division in WT and clock deletion backgrounds under constant light conditions. A clock deletion strain ($\Delta$*kaiBC*) was obtained by deleting the *kaiBC* locus, thus inactivating the KaiABC oscillator. We carried out time-lapse movies under constant 15 µE $m^{-2}$ $s^{-1}$ cool white light, and segmented and tracked thousands of individual cell lineages over multiple generations. The relation between size at birth and size added between birth and division is often indicative of the model controlling when cells decide to divide [14,17]. If size at birth is linearly related to added size with a slope of 1, then the underlying model is called a 'timer', in which cells wait a specific time before division. A slope of -1 is indicative of a 'sizer', where cells divide after reaching a critical size. More generally negative slopes can be categorised as sizer-like while positive slopes represent timer-like strategies [14,43–45]. Alternatively, added size may not correlate with size at birth (slope of 0). Such cells, which grow by a fixed size, irrespective of their birth size, are described as 'adders' [15–17] (Fig. 1). *E. coli* and other bacteria have been shown to obey this adder rule [14]. *S. elongatus* cells are rod-shaped and grow in volume by increasing

their pole-to-pole length, and so cell length is an appropriate measure of cell size. Interestingly, in the WT background, *S. elongatus* cells are best fit by a sizer-like model (slope of -0.63), where the larger they are born, the less length they need to add to reach a target size (red line, Fig. 2A). This effect was less apparent in the clock deletion background, where cells appeared to have a much weaker dependence on birth length (red line, Fig. 2B) (slope of -0.35).

How can a clock cause cells to divide at a specific size? To address this question, we first examined how cell division is affected by the time of day. As has been reported previously [27,33,41] we observed apparent gating of cell division, with fewer cell divisions in the early subjective night in the WT but not in the clock deletion background (Suppl. Fig. 1). We next asked what effect this gating of cell division has on cell cycle times and cell size control. The distribution of cell cycle times was not clearly bimodal (Suppl. Fig. 2), but by clustering cells based on subjective time of birth and cell cycle time (Materials and methods), we found cells lie in two distinct subpopulations (Fig. 2C). Cells born either in late subjective night or early subjective day tend to have shorter cell cycles than those born later in the day in the WT background.

The timing of cell division also affects added length. On average, cells born in late subjective night or early subjective day add less length (red data points in Fig. 2D), as expected from its shorter cell cycle times. Interestingly, within this subpopulation added length decreases with the time of birth (blue line, Fig. 2D). Cells born during subjective

night often divide again before subjective dusk, and this causes a reduction in cell cycle times and added length. By contrast, in the absence of the clock, no two subpopulations are apparent (Fig. 2E) since cell cycle timing does not depend on the time of birth, and added length is constant throughout the day (Fig. 2F).

**A simple model explains the coordination of cell size by the circadian clock**

How does the clock generate two subpopulations with different cell lengths and cell cycle times? To answer this question, we developed a simple model assuming a linear dependence $\Delta(L_0) = a\,L_0 + \Delta_0$ between added length $\Delta$ and birth length $L_0$. The birth-length independent part of added length $\Delta_0$ is a stochastic variable, and the parameter $a$ quantifies its dependence on birth length, which can be estimated by linear regression. Similar models have been used to quantify cell size control of microbes [14,43,44].

In *Synechococcus elongatus* the circadian clock affects the size control. We assume that the clock alters the length-independent part of added length $\Delta_0 = L - (1+a)\,L_0$ by modulating the probability of cell divisions throughout the day. This model implies that the cellular division rate depends on three factors: (i) increase in cell length $\frac{\partial L}{\partial t}$, (ii) the size control $S(\Delta_0)$, and (iii) the gate $G(t)$ imposed by the circadian clock, a periodic function of the time of the day $t$, leading to

$$\textbf{division rate} = \Gamma(L, L_0, \frac{\partial L}{\partial t}, t) = S(L - (1+a)L_0)G(t)\frac{\partial L}{\partial t}. \quad (1)$$

The division rate depends thus on the instantaneous length, length at birth, growth rate and time of the day.

To systematically disentangle the individual components affecting cell division rate, we measured the length-independent part of added length in clock-deletion cells, which do not gate cell divisions ( $G(t)$ =1). We found that it is well fitted by a Gamma distribution (Fig. 3A grey line) implying $S(\Delta_0)$ to be an increasing function of $\Delta_0$ (Fig. 3A black line). Simulations of the resulting stochastic model recover the correct size control in clock-deletion cells (Fig. 3B).

We then used the model to estimate the circadian gate $G(t)$ directly from individual traces of the WT cells via Bayesian inference (Materials and methods). To avoid prior assumptions on the functional form of the gate, we only constrained it to be a smooth, positive and periodic function of the time of day. Our analysis reveals that the circadian gate (Fig. 3C red line) decreases during the middle of the day, effectively delaying cell divisions, but it peaks towards the end of the day where it facilitates cell divisions compared to the clock-deletion strain (dashed grey line).

We also found that elongation rates oscillate in a circadian manner, which is not apparent in the clock deletion background. This highlights that the circadian clock not only affects the decision to divide but it also feeds back on growth [42,46]. To account for

these effects, we measured the mean trend of these oscillations throughout the day (not shown) and incorporated the time-dependent growth rate $\alpha(t)$ into the WT model.

To predict the WT behaviour, we carried out detailed stochastic simulations of the inferred model. In agreement with the experiments (Fig. 2C), the simulations reveal the emergence of differentially timed subpopulations with respect to their birth times (Fig. 3D). We then asked whether the model could also explain the differences in size control observed in the two subpopulations. By clustering the simulation data, we predict added length to decrease throughout the day in the fast subpopulation but not in the slow population (Fig. 3E), in close agreement with the experiments (Fig. 2D).

The model also shows that, as a consequence of the gate imposed by the clock, cells in the fast subpopulation are smaller than in the slow subpopulation. Cells born during subjective day delay division to avoid dividing at night, leading to larger cell sizes (blue cells, Fig. 3E,F). Cells born in the late subjective day speed up to divide before dusk, leading to smaller cells in this subpopulation (red cells, Fig. 3E,F).

Interestingly, cells in the fast subpopulation modify their effective cell size control to more closely conform with the adder principle, but those in the slow subpopulation follow a weak sizer-like trend similar to clock-deletion cells. The stronger dependence of added length on birth-length seen in the overall WT population is thus an emergent

phenomenon arising from differentially timed and sized subpopulations generated by the circadian clock.

**Growth rates of WT and clock-deletion cells are set by light-dark cycles**

Like all other photoautotrophs, *Synechococcus elongatus* did not evolve under constant light. We therefore examined the effects of the circadian clock in growth and division under more physiological environmental conditions. We grew WT and clock-deletion cells under graded 12 hour light and 12 hour dark cycles (12:12 LD) approximating the Earth's cycles of daylight and dark (Materials and methods, Fig. 3A,B). We programmed the light levels such that the amount of light per unit area over a period of 24 hours is identical in constant light and 12:12 LD.

There was no visible growth or cell division in the dark (Fig. 4A,B). As such, the pattern of LD cycles controls the growth rate of both WT and clock deletion cells forbidding cell divisions in the dark. Elongation rates are also set by the level of ambient light during the day. Unlike what we observed in constant light, in graded LD cycles the mean elongation rates of the two strains are nearly identical, and both track the level of ambient light quite accurately (Suppl. Fig. 3, Fig. 4C).

Restricting growth also constrained the distribution of cell cycle times, separating cells into two subpopulations: cells that divide in the same day they were born and cells that

divide only the day after they were born (Fig. 4D). This effect was observed in both WT and clock-deletion cells.

We therefore wondered how the circadian clock interacts with growth cycles imposed by the ambient light levels. By imposing the time-dependent growth rates onto our model of WT and clock-deletion cells, we found that the clock accelerates cell divisions in the fast subpopulations but, interestingly, it delays divisions in the slow subpopulation (blue and red lines, Fig. 4D). In qualitative agreement with this result, we found that in the experiments the change in cell cycle times was indeed negatively correlated with the cell cycle of the two subpopulations. Within the assumptions of our model these findings are explained by the interaction of the clock with the entrained growth rate resulting in an effective gate (dashed grey line, Fig. 4C). In comparison to clock-deletion cells, the effective gate delays cell divisions at dawn but accelerates divisions close to dusk in the WT, highlighting the predictive power of our model. In the following, we answer the question of what role the clock plays for size control.

**The circadian clock modulates cell size in light-dark cycles.**

To understand the effect of varying light levels on cell size control, we used the model to predict the mode of cell size control in the two subpopulations. In these conditions, the growth rate closely follows the ambient light levels implying the system is driven out of steady-state and cell length distributions are not stationary. Interestingly, our model

predicted that WT cells with short cell cycles, i.e. cells that are born and divide within the same day (red dots in Fig. 5A,C, upper panels), add roughly half the length than cells with longer cell cycles, i.e. cells that divide a day after they were born (blue dots, Fig. 5A,C, upper panels). This dependence is well confirmed by the experiments (Fig. 5A,B, lower panels).

Furthermore, the model suggests that cell size controls obeys different rules in the two dynamical subpopulations. Fast dividing cells increment their length with a weak dependence on birth size (Fig. 5A, red line), ie. an adder-like size control, while added length of slow cells increases with birth size (blue line), ie. a timer-like size control. A prediction that was also confirmed by the data (Fig. 5A, lower panel). Clock deletion cells, on the other hand, do not display significant differences in cell size and control between the two subpopulations (Fig. 5C).

WT cells that are born and divide in the same day have cell cycle times that are shorter than corresponding clock deletion cells (Fig. 4D). These cells are mostly born in the first half of the 'daylight' period, but in the WT strain they are born later and have shorter cell cycle times than in the clock deletion strain (red dots, Fig. 4C,D). Consequently, these WT cells with fast cell cycle times end up adding comparatively less length during the cell cycle. On the other hand, cells that divide only in the next day have long cell cycle times and, correspondingly, increment their length by larger amounts (blue dots, Fig. 5C). The synergy of dynamic growth rates and the circadian clock generates an

effective gate (Fig. 4C) which inhibits cell divisions in the early hours of light after dawn. This fact causes WT cells to keep elongating, and when they divide, they are larger than clock deletion cells dividing at the same time. Many of their daughters belong to the subpopulation that divides before dusk, and will be smaller at division owing to their short cell cycle times.

## Discussion

In this work, we have shown how the circadian clock and environmental cycles modulate the underlying division rules of cyanobacteria. We characterised cell size control in constant conditions and showed that the clock generates an apparent sizer-like behaviour that is not present in a clock deletion strain. We hypothesised that circadian gating of cell division generates two subpopulations of cells following different division rules and cell sizes, that cannot be explained using division rules found in other microbes.

We formulated a phenomenological model of the interaction between cell size control and the clock, which confirms that this interaction indeed generates two differently timed and sized subpopulations. Inference suggested that the clock modulates the division rate of cells by increasing the frequency of divisions just before subjective dusk but inhibiting cell division during other times of the day. Our finding thus sheds light on how the circadian clock governs a cell's decision to divide.

Under graded LD cycles, the model predicted that the clock accelerates divisions in the fast subpopulation but delays divisions in the slow subpopulation, a finding which we confirmed experimentally under physiological (12:12) light-dark cycles. By doing so, the clock constricts cell division away from dawn and dusk. This could potentially provide a fitness advantage, by avoiding division during the energetically unfavourable times of early dawn or late dusk.

Examining the relationship between added cell size and birth size has provided valuable insights into how microbes maintain cell size over successive generations [14–17,20]. When cells respond subject to internal or external cues, as in our work, it is challenging to interpret these relationships because the clock modulates cell size control in non-intuitive ways. As we showed, models are needed to disentangle the components affecting cellular decisions throughout the day. Since the clock gates cell division in higher eukaryotes, it will be interesting to observe the influence of the clock in regulating cell size homeostasis in higher eukaryotes, whether in single cells or tissues.

## Materials and methods

### Strains, plasmids and DNA manipulations

*Synechococcus elongatus* WT was obtained from the ATCC cell lines (ATCC® 33912™). A clock deletion strain was generated by insertion of a gentamycin resistance cassette into the ORF of the *kaiBC* operon. The plasmid (a gift from Prof. Erin O'Shea) carrying the

interrupted gene with the antibiotic selection marker was transformed into the WT strain through homologous recombination. Complete allele replacement on all the chromosomal copies was checked through PCR.

| ***S. elongatus* strain** | **Description** | **Antibiotic resistance** | **Source** |
|---|---|---|---|
| 7942_A1 | WT | None | ATCC |
| 7942_A56 | *Δ kaiBC mutant* | Gent$^r$ | This study |
| | | | |
| **Plasmid** | **Description** | **Antibiotic resistance** | **Reference** |
| pUC18-*kaiBC-Gent* | *kaiBC* deleted by the insertion of gentamycin cassette within the ORF | Gent$^r$ | Teng *et al*. [34] |

**Table 1**: Strains and plasmid used in this study.

## Growth conditions

The strains were grown from frozen stocks in BG-11 M media at 30˚C under photoautotrophic conditions with constant rotation. The *Δ kaiBC* strain was supplemented with gentamycin at 2 µg ml$^{-1}$. Light conditions were maintained at approximately 20-25 µE m$^{-2}$ s$^{-1}$ by cool fluorescent light sources. Before the start of each movie acquisition the cultures were kept at exponential phase, and entrained by subjecting the cells to a 12 h light : 12 h dark cycle (12:12 LD).

**Microscopy and sample preparation**

A Nikon Ti-E inverted microscope equipped with the Nikon Perfect Focus System module was used to acquire time-lapse movies of the cells over several days. 2 µl of entrained cultures in exponential phase were diluted to an $OD_{750}$ of 0.15-0.20 and spread on agarose pads. The agarose pads were left to dry and then placed inside a two chambered coverglass (Labtek Services, UK), which was brought under the microscope. The cells were maintained in a 12:12 LD regime for another cycle, and image acquisition was only started after dawn. Illumination for photoautotrophic growth is provided by a circular cool white light LED array (Cairn Research, UK), attached around the condenser lens of the microscope. Light conditions were pre-programmed to run during acquisition. The setup allows for instantaneous and near-continuous light level updates. In constant light experiments, the light level was set at approximately 15 µE $m^{-2}$ $s^{-1}$. In experiments with light-dark cycles, light was set such that the amount of photons per unit area is the same as in constant light over a 24 hour period. The daily profile of solar insolation in the wild was approximated by the function

$$I(t) = \begin{cases} I_{max} \sin\left(\frac{2\pi t}{2T_L}\right) & \text{if } 0 \leq t \leq T_L, \\ 0 & \text{otherwise,} \end{cases}$$

where $T_L$ is the duration of the light period (12 h), and $I_{max} = \frac{24\,A\,\pi}{2\,T_L}$. $A$ ≈ 15 µE $m^{-2}$ $s^{-1}$ is light level in constant light, and so $I_{max}$ ≈ 47 µE $m^{-2}$ $s^{-1}$ in 12:12 LD. Data acquisition was controlled through the software Metamorph (Molecular Devices, California). At each time point, phase contrast and fluorescent images using the filter set 41027-Calcium Crimson (Chroma Technology, Vermont) and a CoolSNAP HQ2 camera

(Photometrics, Arizona) were acquired. The fluorescent image is used to improve image segmentation. In constant light, images were acquired every 45 minutes. In light-dark conditions, images were acquired every hour during the day. The reduction in the frequency of acquisition is implemented to avoid photo toxicity when the light levels are very low and growth is slow. The frequency of acquisition was therefore further reduced in the dark. Finally, the light levels were updated after each stage position is visited and acquired. In between time points, the light levels were updated every 2 minutes. All experiments used a 100X objective. This protocol was adapted from Young *et al.* [47].

## Quantitative analysis

### Segmentation and cell length

All images were segmented and tracked using a modified version of Schnitzcells [47]. The segmentation algorithm is performed on a combined fluorescent-phase contrast image. The fluorescent image is acquired in a range of red wavelengths, and so it collects the cells' auto-fluorescence. Since *S. elongatus* cells are rod shaped, cell size is proportional to cell length. Cell length is defined as the length of the semi-major axis of the segmented cell shapes.

### Defining subjective time of birth and division under constant light

Cells were entrained by 12:12 LD cycles (step cycles) before acquisition. We consider subjective dawn to occur immediately after the lights are switched on following the last

12 h dark pulse. Subsequent subjective dawn times are considered to occur multiples of 24 h later. We define subjective dusk times to occur 12 h after subjective dawn.

**Subpopulation clustering**

For each tracked single cell that completed a cell cycle during image acquisition, we extracted distributions of time of birth, time of division, length at birth, length at division, added length and cell cycle time. Distributions of time of birth and cell cycle time revealed two distinct peaks (Fig. 2C). We extracted the cells that lie in each subpopulation by clustering with a two-component Gaussian mixture model using likelihood-ratio criterion.

**Estimating cell size control in the clock-deletion strain**

We parameterized the dynamic model of the size control of the clock-deletion strain by first estimating the slope $a$ through a linear regression. We then estimate the residuals of the regression via $\Delta_0 = L - (1+a)\,L_0$, and fit these data by a Gamma distribution $p(\Delta_0)$. The size control hazard $S(\Delta_0)$ is obtained as the ratio of this distribution and its survival function giving the relation

$$S(\Delta_0) = \frac{p(\Delta_0)}{\int_{\Delta_0}^{\infty} \mathrm{d}x\, p(x)}.$$

This procedure was used to fit the size control Fig. 2-5 from the corresponding experiments of clock-deletion cells.

**Inference of the circadian gate function from single-cell data**

To determine the gate function, we need to estimate the likelihood of the circadian gate function. The probability for a single cell to divide born at time $t_0$ after cell cycle time $\tau$ is a product of the probability of cell division $\Gamma(L(t_0+\tau), L(t_0), \frac{\partial L}{\partial \tau}, t_0+\tau)d\tau$ and the probability that the given cell has not divided before that time. The result is

$$\mathrm{P}(\tau|\mathbf{L}(t)_{t\in[t_0,t_0+\tau)}, \frac{\partial L}{\partial \tau}, t_0) = \Gamma(L(t_0+\tau), L(t_0), \frac{\partial L}{\partial \tau}, t_0+\tau) e^{-\int_0^{\tau} \mathrm{d}\tau' \, \Gamma(L(t_0+\tau'), L(t_0), \frac{\partial L}{\partial \tau'}, t_0+\tau')}.$$

This expression not only depends on the whole single-cell trajectory of length but also on its derivative with respective to cell age $\tau'$.

Because derivatives are difficult to estimate from single-cell data, we focus on the likelihood for a cell to divide at a specific length, which can be obtained by a change of variable. Using Eq. (1) in the above equation, we obtain the probability of a cell to divide at a length $L$,

$$\mathrm{P}(L(t_0+\tau)|\mathbf{L}(t)_{t\in[t_0,t_0+\tau)}, t_0) = G(t_0+\tau)S(L(\tau)-(1+a)L(t_0)) e^{-\int_{L(t_0)}^{L(t_0+\tau)} \mathrm{d}x \, G(t_0+\tau'(x))S(x-(1+a)L(t_0))},$$

a quantity that is independent of the length derivatives but depends on cell age $\tau'(L)$. Since cell length strictly increases in almost all of the observed single-cell traces, we estimated this quantity by interpolating cell age against cell length measurements for each cell using a cubic B-spline and evaluated the resulting integral in the above equation numerically.

The likelihood of the gate function given $N$ single-cell observations is then given by

$$\mathcal{L}(\mathbf{G}(t)_{t\in[0,24)}|\{t_{0,i},\mathbf{L}_i(t)_{t\in[t_{0,i},t_{0,i}+\tau_i]}\}_{i=1,..,N}) = \prod_{i=1}^{N} \mathrm{P}(L_i(t_{0,i}+\tau_i)|\mathbf{L}_i(t)_{t\in[t_{0,i},t_{0,i}+\tau_i)},t_{0,i}).$$

We parameterized the gate function $G(t) = exp(B(t))$, a positive function with arguments taken modulo 24 hours, by a cubic B-spline $B(t)$ with 12 knots 0,2,...,22 and periodic boundary conditions as implemented by the Julia library *Interpolations* [48]. The spline was evaluated at the knots and we sampled the posterior distributions using an adaptive Gibbs-sampler implemented in the Julia library *Mamba* [49]. The result of this inference is shown in Fig. 2C.

## Acknowledgements

PT gratefully acknowledges support by The Royal Commission for the Exhibition of 1851.

## References

1. Wood, E. & Nurse, P. Sizing up to divide: mitotic cell-size control in fission yeast. *Annu. Rev. Cell Dev. Biol.* **31,** 11–29 (2015).
2. Amodeo, A. A. & Skotheim, J. M. Cell-size control. *Cold Spring Harb. Perspect. Biol.* **8,** a019083 (2016).
3. Chien, A.-C., Hill, N. S. & Levin, P. A. Cell size control in bacteria. *Curr. Biol.* **22,** R340–9 (2012).
4. Gonzalez, N., Vanhaeren, H. & Inzé, D. Leaf size control: complex coordination of cell division and expansion. *Trends Plant Sci.* **17,** 332–340 (2012).
5. Cooper, S. Control and maintenance of mammalian cell size. *BMC Cell Biol.* **5,** 35 (2004).
6. Orskov, J. Method for the isolation of bacteria in pure culture from single cells and

procedure for the direct tracing of bacterial growth on a solid medium. *J. Bacteriol.* **7,** 537–549 (1922).

7. Kelly, C. D. & Rahn, O. The growth rate of individual bacterial cells. *J. Bacteriol.* **23,** 147–153 (1932).
8. Turner, J. J., Ewald, J. C. & Skotheim, J. M. Cell size control in yeast. *Curr. Biol.* **22,** R350–9 (2012).
9. Osella, M., Nugent, E. & Lagomarsino, M. C. Concerted control of Escherichia coli cell division. *Proc. Natl. Acad. Sci. U. S. A.* **111,** 3431–3435 (2014).
10. Wang, P., Hayden, S. & Masui, Y. Transition of the blastomere cell cycle from cell size-independent to size-dependent control at the midblastula stage in Xenopus laevis. *J. Exp. Zool.* **287,** 128–144 (2000).
11. Sveiczer, A., Novak, B. & Mitchison, J. M. The size control of fission yeast revisited. *J. Cell Sci.* **109 ( Pt 12),** 2947–2957 (1996).
12. Nobs, J.-B. & Maerkl, S. J. Long-term single cell analysis of S. pombe on a microfluidic microchemostat array. *PLoS One* **9,** e93466 (2014).
13. Iyer-Biswas, S. *et al.* Scaling laws governing stochastic growth and division of single bacterial cells. *Proc. Natl. Acad. Sci. U. S. A.* **111,** 15912–15917 (2014).
14. Sauls, J. T., Li, D. & Jun, S. Adder and a coarse-grained approach to cell size homeostasis in bacteria. *Curr. Opin. Cell Biol.* **38,** 38–44 (2016).
15. Campos, M. *et al.* A constant size extension drives bacterial cell size homeostasis. *Cell* **159,** 1433–1446 (2014).
16. Amir, A. Cell Size Regulation in Bacteria. *Phys. Rev. Lett.* **112,** (2014).
17. Taheri-Araghi, S. *et al.* Cell-size control and homeostasis in bacteria. *Curr. Biol.* **25,** 385–391 (2015).

18. Soifer, I., Robert, L. & Amir, A. Single-cell analysis of growth in budding yeast and bacteria reveals a common size regulation strategy. *Curr. Biol.* **26,** 356–361 (2016).

19. Deforet, M., van Ditmarsch, D. & Xavier, J. B. Cell-size homeostasis and the incremental rule in a bacterial pathogen. *Biophys. J.* **109,** 521–528 (2015).

20. Yu, F. B. *et al.* Long-term microfluidic tracking of coccoid cyanobacterial cells reveals robust control of division timing. *BMC Biol.* **15,** 11 (2017).

21. Kuwano, K. *et al.* Growth and cell cycle of Ulva compressa (Ulvophyceae) under LED illumination. *J. Phycol.* **50,** 744–752 (2014).

22. Bišová, K. & Zachleder, V. Cell-cycle regulation in green algae dividing by multiple fission. *J. Exp. Bot.* **65,** 2585–2602 (2014).

23. Nishihama, R. & Kohchi, T. Evolutionary insights into photoregulation of the cell cycle in the green lineage. *Curr. Opin. Plant Biol.* **16,** 630–637 (2013).

24. Nozue, K. *et al.* Rhythmic growth explained by coincidence between internal and external cues. *Nature* **448,** 358–361 (2007).

25. Doherty, C. J. & Kay, S. A. Circadian control of global gene expression patterns. *Annu. Rev. Genet.* **44,** 419–444 (2010).

26. Sweeney, B. M. & Woodland Hastings, J. Rhythmic cell division in populations of Gonyaulax polyedra. *J. Protozool.* **5,** 217–224 (1958).

27. Mori, T., Binder, B. & Johnson, C. H. Circadian gating of cell division in cyanobacteria growing with average doubling times of less than 24 hours. *Proc. Natl. Acad. Sci. U. S. A.* **93,** 10183–10188 (1996).

28. Bieler, J. *et al.* Robust synchronization of coupled circadian and cell cycle oscillators in single mammalian cells. *Mol. Syst. Biol.* **10,** 739 (2014).

29. Feillet, C. *et al.* Phase locking and multiple oscillating attractors for the coupled mammalian

clock and cell cycle. *Proc. Natl. Acad. Sci. U. S. A.* **111,** 9828–9833 (2014).

30. Matsuo, T. *et al.* Control mechanism of the circadian clock for timing of cell division in vivo. *Science* **302,** 255–259 (2003).
31. Kuan, D., Duff, S., Posarac, D. & Bi, X. Growth optimization of Synechococcus elongatus PCC7942 in lab flasks and a 2-D photobioreactor. *Can. J. Chem. Eng.* **93,** 640–647 (2015).
32. Chabot, J. R., Pedraza, J. M., Luitel, P. & van Oudenaarden, A. Stochastic gene expression out-of-steady-state in the cyanobacterial circadian clock. *Nature* **450,** 1249–1252 (2007).
33. Dong, G. *et al.* Elevated ATPase activity of KaiC applies a circadian checkpoint on cell division in Synechococcus elongatus. *Cell* **140,** 529–539 (2010).
34. Teng, S.-W., Mukherji, S., Moffitt, J. R., de Buyl, S. & O'Shea, E. K. Robust circadian oscillations in growing cyanobacteria require transcriptional feedback. *Science* **340,** 737–740 (2013).
35. Rust, M. J., Markson, J. S., Lane, W. S., Fisher, D. S. & O'Shea, E. K. Ordered phosphorylation governs oscillation of a three-protein circadian clock. *Science* **318,** 809–812 (2007).
36. Cohen, S. E. & Golden, S. S. Circadian rhythms in cyanobacteria. *Microbiol. Mol. Biol. Rev.* **79,** 373–385 (2015).
37. Ito, H. *et al.* Autonomous synchronization of the circadian KaiC phosphorylation rhythm. *Nat. Struct. Mol. Biol.* **14,** 1084–1088 (2007).
38. Markson, J. S., Piechura, J. R., Puszynska, A. M. & O'Shea, E. K. Circadian control of global gene expression by the cyanobacterial master regulator RpaA. *Cell* **155,** 1396–1408 (2013).
39. Diamond, S., Jun, D., Rubin, B. E. & Golden, S. S. The circadian oscillator in Synechococcus elongatus controls metabolite partitioning during diurnal growth. *Proc. Natl. Acad. Sci. U. S. A.* **112,** E1916–25 (2015).
40. Pattanayak, G. K., Phong, C. & Rust, M. J. Rhythms in energy storage control the ability of

the cyanobacterial circadian clock to reset. *Curr. Biol.* **24,** 1934–1938 (2014).

41. Yang, Q., Pando, B. F., Dong, G., Golden, S. S. & van Oudenaarden, A. Circadian gating of the cell cycle revealed in single cyanobacterial cells. *Science* **327,** 1522–1526 (2010).
42. Lambert, G., Chew, J. & Rust, M. J. Costs of Clock-Environment Misalignment in Individual Cyanobacterial Cells. *Biophys. J.* **111,** 883–891 (2016).
43. Tanouchi, Y. *et al.* A noisy linear map underlies oscillations in cell size and gene expression in bacteria. *Nature* **523,** 357–360 (2015).
44. Priestman, M., Thomas, P., Robertson, B. D. & Shahrezaei, V. Mycobacteria modify their cell size control under sub-optimal carbon sources. *Front Cell Dev Biol* **5,** (2017).
45. Modi, S., Vargas-Garcia, C. A., Ghusinga, K. R. & Singh, A. Analysis of Noise Mechanisms in Cell-Size Control. *Biophys. J.* **112,** 2408–2418 (2017).
46. Martins, B. M., Das, A. K., Antunes, L. & Locke, J. C. Frequency doubling in the cyanobacterial circadian clock. *Mol. Syst. Biol.* **12,** 896 (2016).
47. Young, J. W. *et al.* Measuring single-cell gene expression dynamics in bacteria using fluorescence time-lapse microscopy. *Nat. Protoc.* **7,** 80–88 (2011).
48. *Interpolations: Fast, continuous interpolation of discrete datasets in Julia*.
49. Smith, B. J. et al. *Mamba: Markov chain Monte Carlo for Bayesian analysis in Julia*.

## Figures

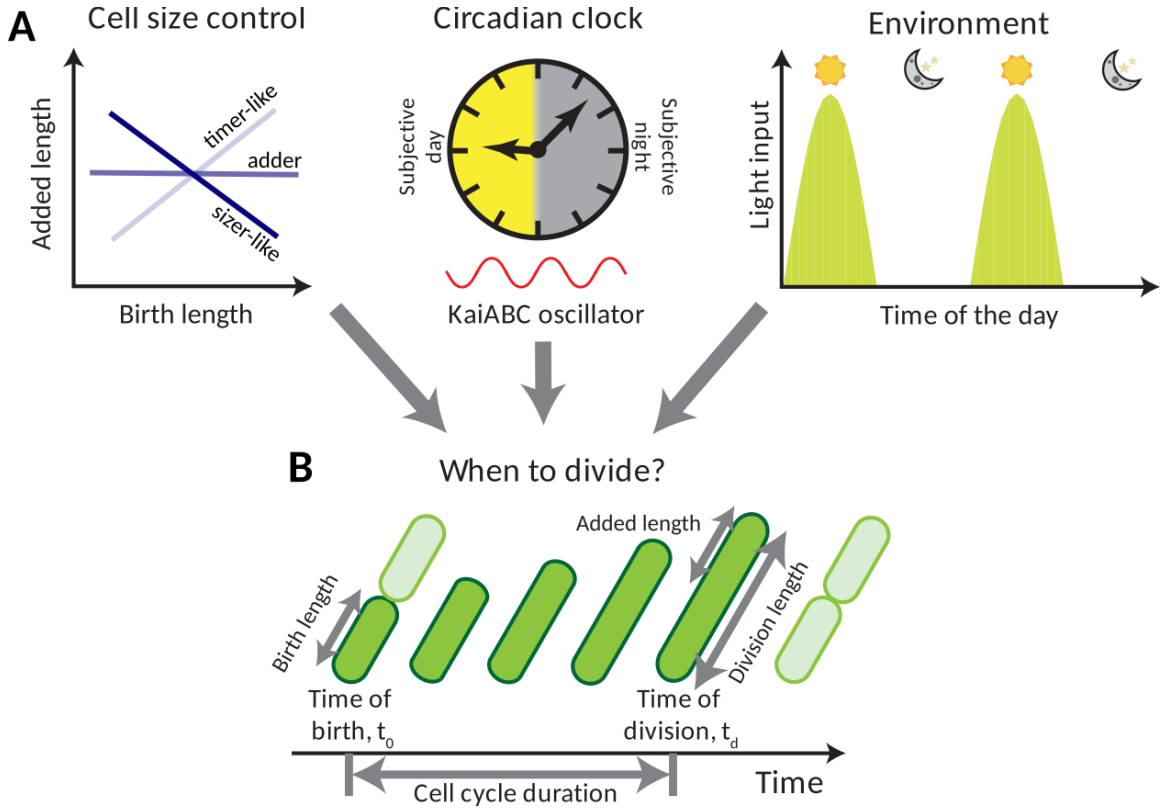


**Figure 1: Orchestration of cell growth and divisions in cyanobacteria.**

**(A)** Cell division in cyanobacteria depends on cell-individual factors such as cell size control and the circadian clock and the environment through light inputs. **(B)** To quantify the impact of these component on a cell's decision to divide, we quantified timings of birth and divisions and the increase in cell length using time-lapse microscopy.

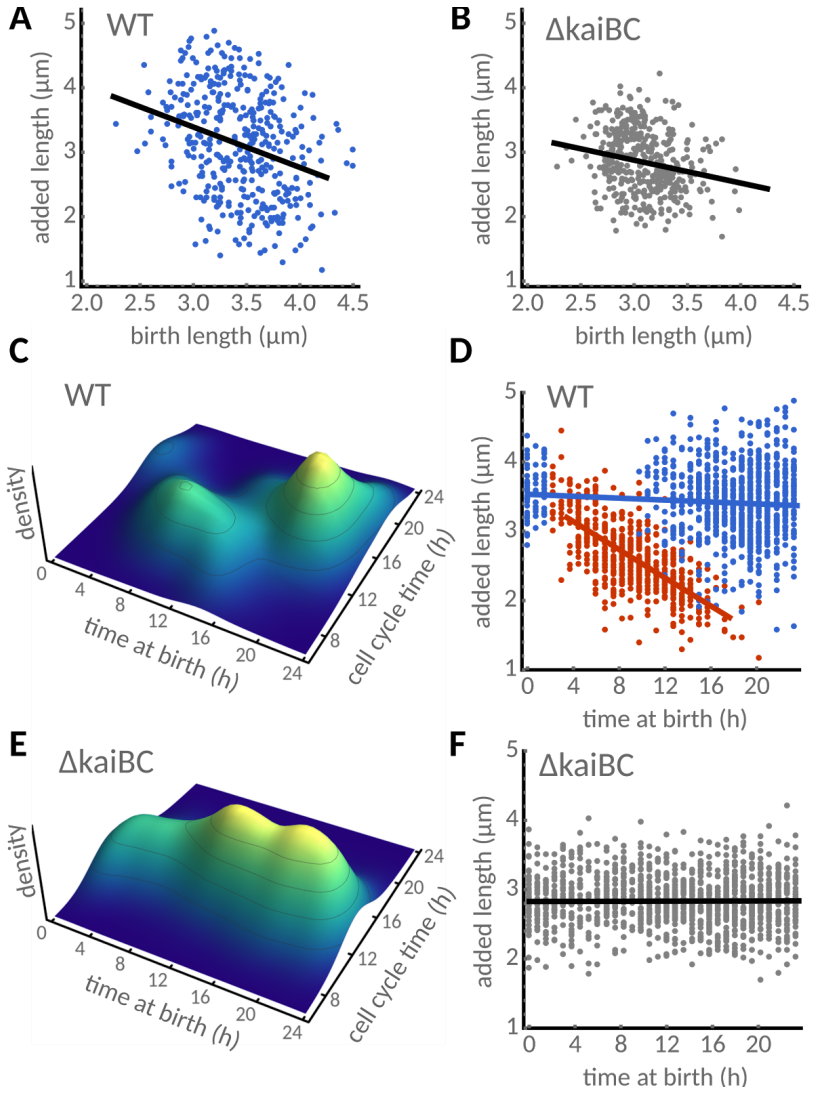


**Figure 2: Coordination of cell size control by the circadian clock in *Synechococcus elongatus* under constant light. (A)** Wild type cells (WT) follow an apparent sizer principle, adding shorter lengths the longer their birth length is (black line, linear regression with slope of -0.63). 1529 individual cells from 3 independent experiments were analysed. **(B)** Cell size control in a clock deletion mutant (ΔkaiBC) follows more closely an adder principle, with a lesser dependence of added length on birth length (black line, slope of -0.35). 1348 individual cells from 3 independent experiments were used. **(C)** The dynamics of WT cells dynamics exhibits two distinct subpopulations: cells born late in their subjective day have

longer cell cycles than cells born earlier. **(D)** Clustering of the two subpopulations reveals that added lengths of cells born earlier in the day (red dots) decrease during the day, while added length is constant for cells born towards the end (blue dots). Red and blue lines show linear regression of the two subpopulations. **(E-F)** In populations of the clock-deletion cells, cell cycle times and added length do not depend on the time of day.

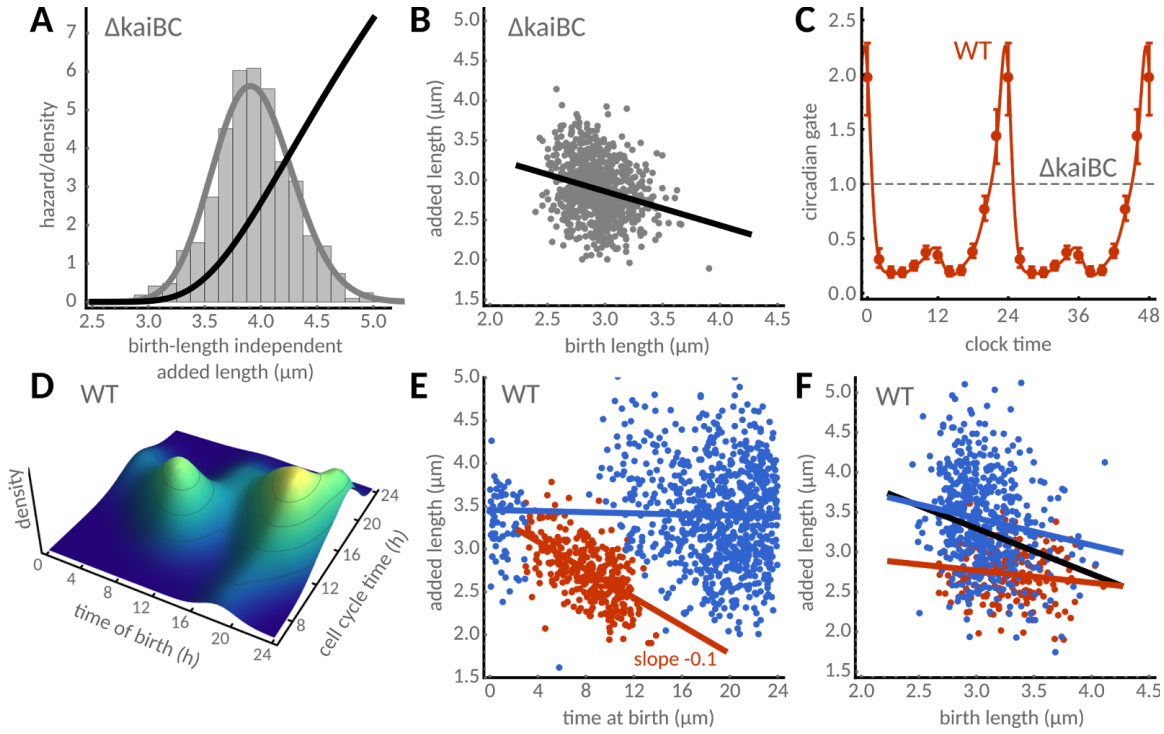


**Figure 3: A simple model explains the emergence of the two subpopulations.** Cell division rate is coordinated by growth rate, size control and coordination by the circadian clock. **(A)** Distribution of the birth-length independent added length ( $\Delta_0$ , grey bars) is fit by a Gamma distribution (grey solid line), the corresponding cell size control hazard $S(\Delta_0)$ increases with length (solid black line). **(B)** The model reproduces the size control in the clock-deletion strain (slope -0.35, compare Fig. 2B). **(C)** Bayesian inference from single-cell traces reveals circadian gating of cell divisions throughout the day in the WT. The gate function, $G(t)$, parameterized by a positive periodic spline (red line, error bars denote 95% credible interval at knots), decreases the division probability in the middle of the day but peaks towards the end of the day compared to the clock-deletion background (dashed grey line). **(D)** Simulations using the inferred gate predict the emergence of two subpopulations in close agreement with experimental data (Fig. 2D). **(E)** Clustering of the simulated data also predicts added length to decrease during the day in the fast subpopulation but not in the

slow population (red line, slope -0.08). **(F)** The model predicts larger cell lengths in the slow subpopulation (blue dots) compared to clock-deletion cells with a similar decrease with birth length (blue line, slope -0.34), and smaller cell lengths in the fast subpopulation (red dots) with a weaker dependence on birth length (red line, slope -0.15). The difference in cell size of the two populations explains the strong dependence of added length on birth length seen in WT cells (black line, slope -0.57).

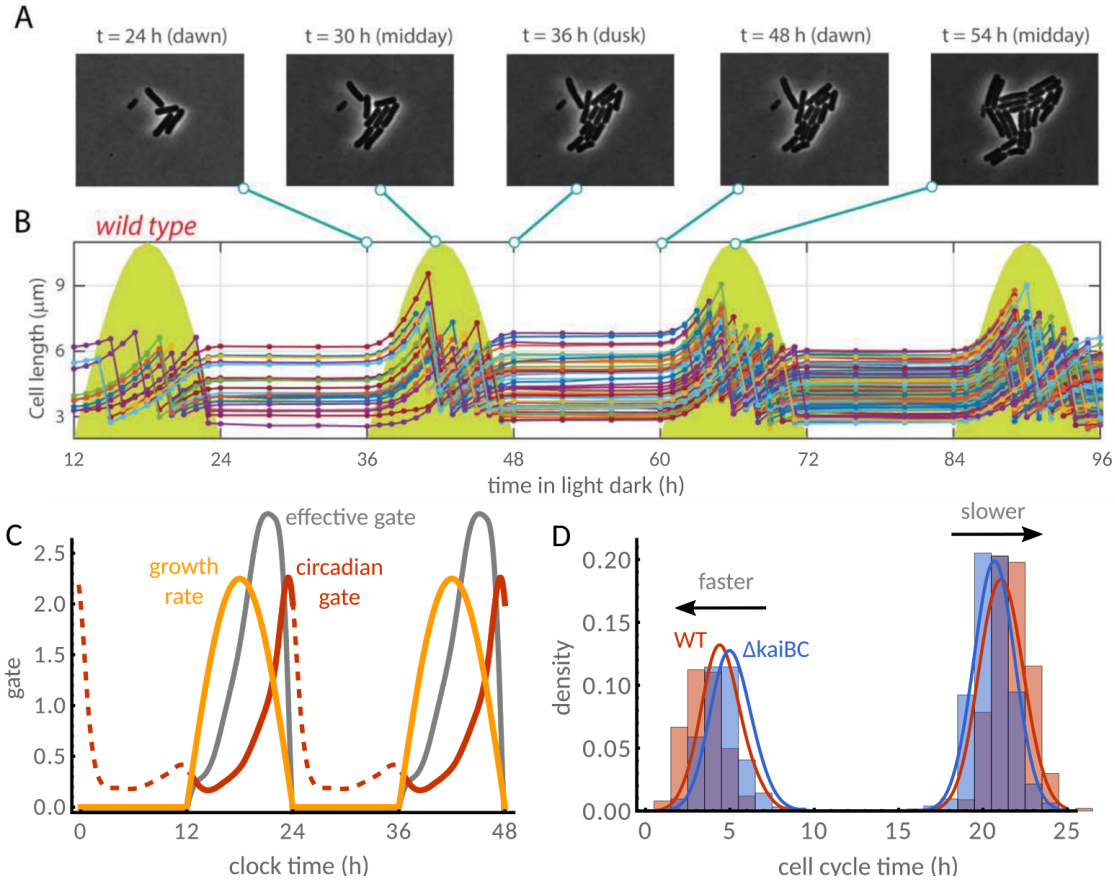


**Figure 4: The rate of growth under light-dark (LD) cycles is determined by the light profile for WT and clock deletion cells. (A)** Phase contrast images of a WT micro-colony under graded 12:12 LD cycles reveal periods of growth followed by periods of stagnation between dusk and dawn. **(B)** Length profile of single cells (coloured lines) in a time-lapse movie. Cell growth and divisions are suspended in the dark and rises slowly rises when the lights turn on. The yellow shades represent the light levels imposed on the cells during the experiment (maximum at midday is approximately 47 μE $m^{-2}$ $s^{-1}$). **(C)** Growth rates of WT (yellow line) and clock-deletion cells closely follow the imposed light profiles. Growth rate (yellow) and circadian clock (red) provide an effective gate (grey line) shifting cell division towards the end of the day. **(D)** The light conditions split cells into two subpopulations: those that complete a full cycle during the period when the lights are on (short cell cycle times), and

those that must wait until the next day to complete a cell cycle (long cell cycle times). Our model shows that the fast WT population (red line) is faster than in the clock-deletion mutant (blue line), but the slow subpopulation is faster in the clock deletion background. This prediction is confirmed by experimental histograms of cell cycle times for WT (1007 cells from two experiments) and clock deletion cells (1258 cells from two experiments).

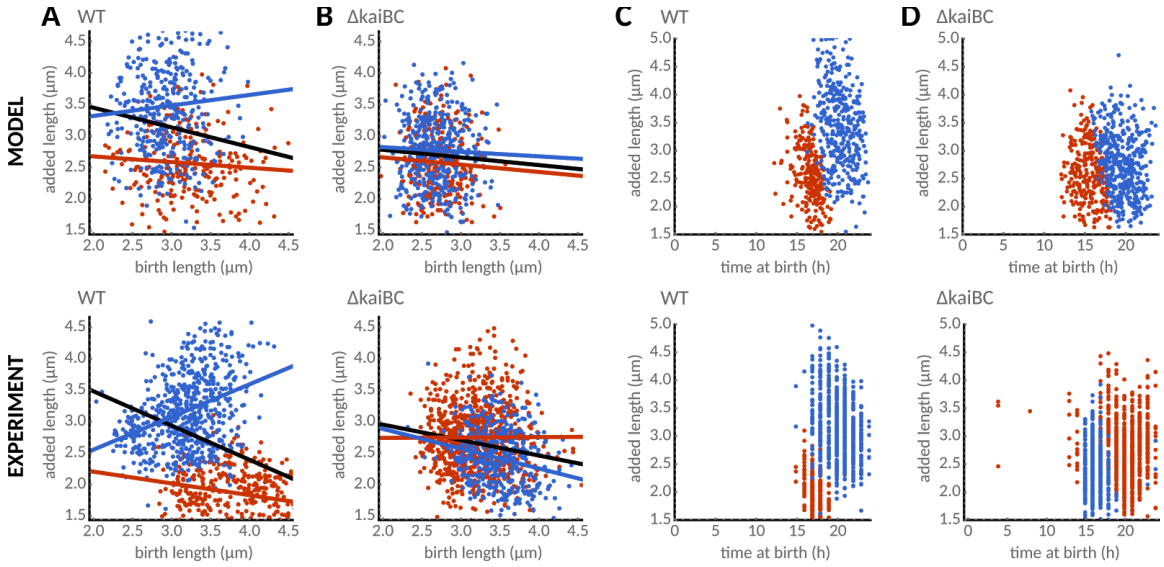


**Figure 5: The circadian clock modulates the size control in 12:12 LD cycles. (A)** The model (upper panel) predicts that the two subpopulations of cells in the WT (short cell cycles, red) and long cell cycles obey different cell size control strategies. Fast dividing cells obey an adder-like principle (red line from linear regression, -0.09) while slowly dividing cells show a timer-like size control (blue line, slope +0.17), which is well confirmed by the experiments (lower panel, slope blue line +0.52, slope red line -0.19, 1007 cells from 2 experiments). **(B)** In the clock-deletion population (1258 cells from 2 experiments), slow and fast cells obey similar trends in size control compared to the overall population. **(C)** Cells that divide in the same day they were born (red dots) are born earlier in the day on average, and increment by smaller lengths than cells whose cell cycle spans to the next day (blue circles). **(D)** In contrast to the WT, in the clock deletion mutant, both subpopulations increment approximately the same length to their birth lengths.

## Supplementary figures

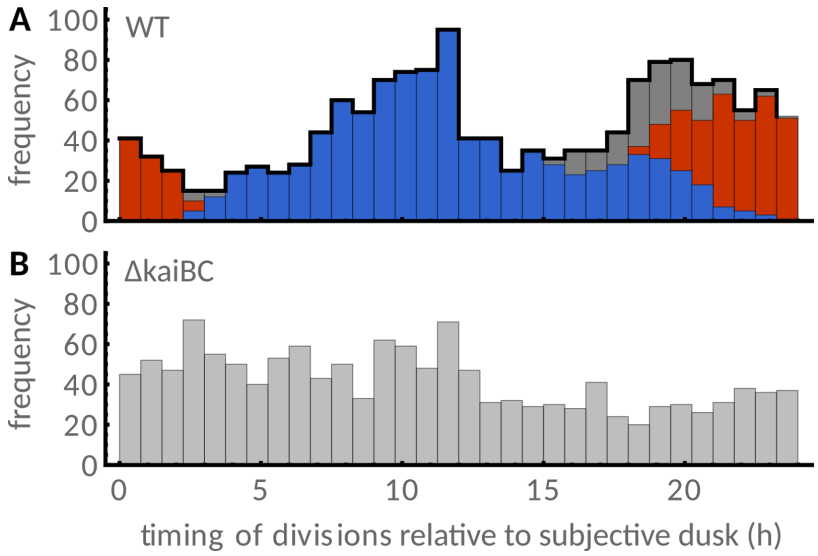


**Supplementary Figure 1: Distribution of division times in constant light. (A)** Division times in WT are gated and display a bimodal division time distribution (black line). Clustering of subpopulations shows that fast cells (red histograms) divide mostly before dusk at the end of the subjective day while slow cells (blue histogram) divide around subjective dawn (Materials and methods). **(B)** In the clock mutant (bottom) the distribution is more uniform. Sample sizes as in Fig. 2.

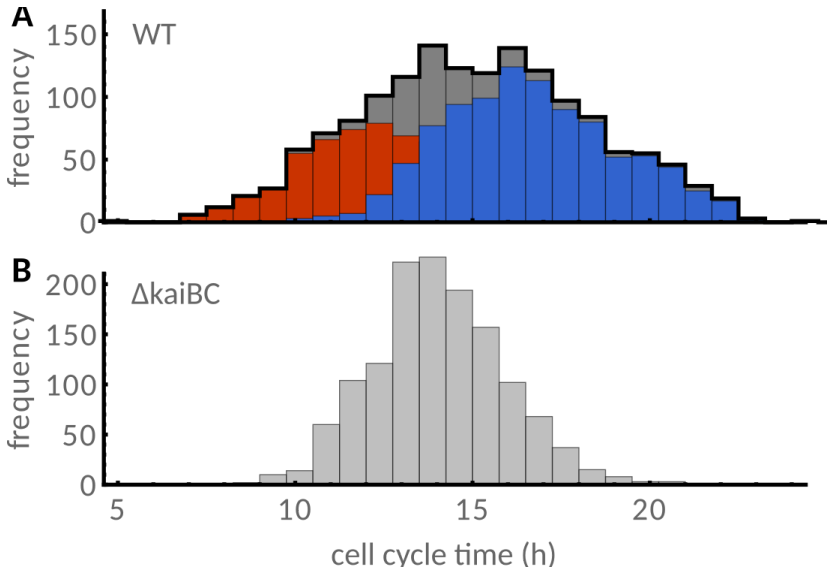


**Supplementary Figure 2: Distribution of cell cycle times in constant light. (A)** Histograms show overlapping subpopulations with shorter (red) and longer cell cycle times (blue), respectively. The overall distribution is only weakly bimodal (black line). **(B)** In clock deletion cells, histograms of cell cycle times is unimodal and narrower than in the wild type. Sample sizes as in Fig. 2.

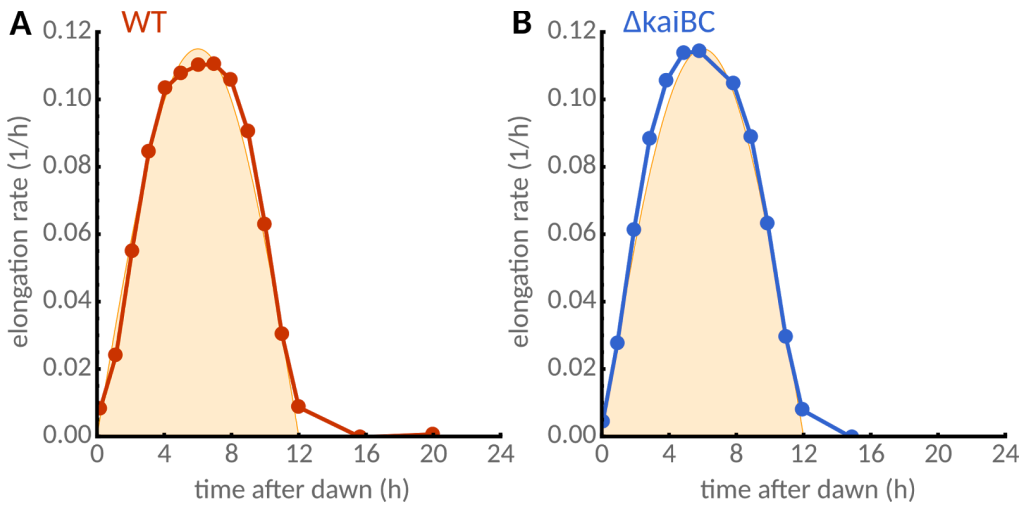


**Supplementary Figure 3: Exponential elongation rates in 12:12 LD cycles. (A)** The mean elongation rate of WT cells (red dots) in a 24 h period closely follows the imposed light profiles (yellow shade). **(B)** The mean elongation rate of clock deletion cells (blue dots) is almost identical to the WT under these conditions and is also determined by the light profile.